Superlattices and Microstructures 93 (2016) 27–31

Contents lists available at ScienceDirect

Superlattices and Microstructures

journal homepage: www.elsevier.com/locate/superlattices

Residual stress in AlN films grown on sapphire substrates by molecular beam epitaxy

Xin Rong [a], Xinqiang Wang [a, b, *], Guang Chen [a], Jianhai Pan [a], Ping Wang [a], Huapeng Liu [a], Fujun Xu [a], Pingheng Tan [c], Bo Shen [a, b, **]

[a] State Key Laboratory of Artificial Microstructure and Mesoscopic Physics, School of Physics, Peking University, Beijing 100871, China
[b] Collaborative Innovation Center of Quantum Matter, Beijing, China
[c] State Key Laboratory for Superlattices and Microstructures, Institute of Semiconductors, Chinese Academy of Sciences, Beijing 100083, China

ARTICLE INFO

Article history:
Received 22 February 2016
Received in revised form 27 February 2016
Accepted 29 February 2016
Available online 2 March 2016

Keywords:
Raman scattering
Aluminium nitride
Molecular beam epitaxy

ABSTRACT

Residual stress in AlN films grown by molecular beam epitaxy (MBE) has been studied by Raman scattering spectroscopy. A strain-free Raman frequency and a biaxial stress coefficient for E_2(high) mode are experimentally determined to be 657.8 ± 0.3 cm^{-1} and 2.4 ± 0.2 cm^{-1}/GPa, respectively. By using these parameters, the residual stress of a series of AlN layers grown under different buffer layer conditions has been investigated. The residual compressive stress is found to be obviously decreased by increasing the Al/N beam flux ratio of the buffer layer, indicating the generation of tensile stress due to stronger coalescence of AlN grains, as also confirmed by the *in-situ* reflection high energy electron diffraction (RHEED) monitoring observation. The stronger coalescence does lead to improved quality of AlN films as expected.

1. Introduction

Recently, AlGaN-based quantum devices have attracted much research attention in the areas of electrical engineering, material science, and physics due to the numerous potential applications such as ultraviolet solid-state light sources, solar-blind photodetectors and so on [1,2]. Among the III-nitride semiconductors, AlN is always regarded as a preferred device substrate or template material for crack-free fabrication. Up to now, great progress has been made for the growth of either bulk AlN or AlN templates [3–6]. However, the device performance is still greatly limited by the strain-induced bending or cracks in thick AlN films commonly grown by hetero-epitaxy on sapphire, Si or SiC substrates [7,8]. In this sense, residual stress analysis in layered structures is of great importance for understanding the mechanical properties of AlN films and helps to adjust the strain status for crystalline quality improvement. Among all the techniques, Raman scattering spectroscopy provides a contactless, non-destructive and sensitive tool to characterize the stress distribution, making it an essential and potential way for residual stress analysis [9]. Generally, the biaxial stress distribution can be easily acquired by the linear

* Corresponding author. State Key Laboratory of Artificial Microstructure and Mesoscopic Physics, School of Physics, Peking University, Beijing 100871, China.
** Corresponding author. State Key Laboratory of Artificial Microstructure and Mesoscopic Physics, School of Physics, Peking University, Beijing 100871, China.
E-mail addresses: wangshi@pku.edu.cn (X. Wang), bshen@pku.edu.cn (B. Shen).

http://dx.doi.org/10.1016/j.spmi.2016.02.050
0749-6036/

dependence of biaxial stress on E_2(high) phonon frequency using the obtained strain-free Raman frequency and biaxial stress coefficient. Some efforts have been performed on this issue and both theoretical and experimental results have been explored [10–13]. However, most reports focused on MOCVD-grown or HVPE-grown templates which somehow disagreed with the theoretical values and the contradictions were not well explained. Few reports are available to precisely determine the above parameters from AlN films grown by molecular beam epitaxy (MBE).

MBE supplies us a way to obtain atomically flat and high-purity AlN templates. The avoidance of oxygen contamination is of great importance towards the high-quality AlGaN quantum wells [14,15]. In the early work, we have obtained a much broad growth window for droplet-free AlN films with step-flow feature [16]. But the crystalline quality can still be further improved through studying the strain states in the epi-layers. In this work, the crystalline quality of MBE-grown AlN films was improved by increasing the Al/N beam flux ratio during AlN buffer layer growth. Residual stress analysis showed that this improvement originated from a stronger AlN grains coalescence for higher Al/N ratio. This analysis is based on the obtained values of the biaxial stress coefficient and strain-free Raman frequency for E_2(high) mode, which have been experimentally determined in this work and found to be well in accord with the theoretically predicted values.

2. Experimental

The growth of AlN films was performed on the 2-inch c-plane sapphire substrates by plasma-assisted MBE system (SVTA). Reflection high energy electron diffraction (RHEED) and an optical reflection spectrometer are used to *in-situ* monitor the whole growth process. Sapphire substrate was first thermally cleaned at 1000 °C for an hour. Then, nitridation was performed at 800 °C for half an hour, leading to the formation of very thin AlN layer on the surface. AlN layers were then deposited by using low temperature AlN buffer layer. To evaluate the residual strain, tens of samples were selected at different growth conditions such as varied growth temperature, Al/N ratio and thickness as ever reported [16]. To study the effect of buffer layer growth condition on quality improvement, five samples with common structure of 30-nm-thick AlN buffer layers and 360-nm-thick AlN top layers were grown. Another sample without buffer layer, as a reference, was also grown. All the growth process is kept the same except that the Al/N ratio changes monotonically during the buffer layer growth. The lattice constants of the AlN films have been determined by high-resolution X-ray diffraction (XRD) measurements using $K\alpha_1$ ($\lambda = 0.15$ nm) radiation. Residual stress was estimated by Raman spectroscopy at room temperature in z(x, x)-z backscattering geometry using a laser excitation source at a wavelength of 514 nm.

3. Results and discussion

To study the biaxial residual stress in hexagonal AlN by Raman scattering measurement, one usually pays attention to E_2(high) mode since it corresponds to atomic oscillations in the c-plane [17]. Two parameters are important to study stress, i.e. strain-free Raman frequency for E_2(high) mode and the Raman biaxial stress coefficient (k). The in-plane residual stress (σ_a) can be derived by using $\sigma_a = k^{-1}\Delta\omega[E_2(high)]$, where $\Delta\omega[E_2(high)]$ is the strain-induced Raman frequency shift for E_2(high) mode. To determine the biaxial stress coefficient as accurate as possible, Raman scattering measurements were performed on a large number of samples grown on sapphire substrates by MBE. Fig. 1(a) shows a typical Raman scattering spectrum for AlN layer grown on the sapphire substrate, where several scattering peaks are observed. The peaks located at 657 and 890 cm^{-1}

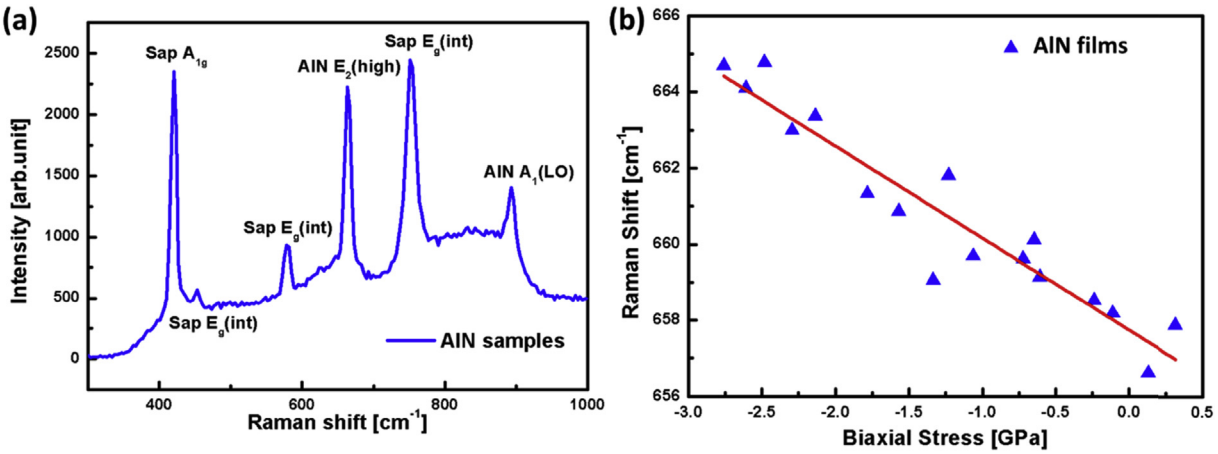

Fig. 1. (a) A typical Raman spectrum of MBE-grown AlN films on sapphire. Visible are the E_2(high) and A_1 (LO) modes in AlN films as well as A_{1g} and E_g(int) modes in sapphire substrate. (b) Raman frequencies of E_2(high) phonon mode as a function of residual biaxial stress. The red line shows a linear fit to the data, which gives a strain-free phonon frequency of 657.8 ± 0.3 cm^{-1} and a biaxial stress coefficient of 2.4 ± 0.2 $\boldsymbol{cm^{-1}/GPa}$ for the E_2(high) mode. (For interpretation of the references to colour in this figure legend, the reader is referred to the web version of this article.)

are assigned to the E_2(high) and A_1(LO) modes, respectively [17]. Other peaks located at 578 and 751 cm^{-1} are two scattering peaks from E_g(int) phonon modes, while the one located at 418 cm^{-1} is A_{1g} mode of sapphire substrate [18,19]. The typical line widths of scattering peaks from the E_2(high) mode of the AlN films are 5–8 cm^{-1}, which indicates good crystalline quality considering that the thickness of AlN layers is less than 400 nm.

Then, residual stress in AlN layer can be estimated by using XRD measurement, where the stress is derived from the deformation of lattice constant. The out-of-plane strain (ε_c) can be obtained by using $\varepsilon_c = (c - c_0)/c_0$, where c is measured lattice constant and $c_0 = 0.49792$ nm is the lattice constant of free-standing AlN [11]. Assuming Hooke's law for elastic deformation, there is $\varepsilon_c/\varepsilon_a = -2\nu/(1-\nu)$, and the biaxial stress σ_a can be obtained by:

$$\sigma_a = \left(C_{11} + C_{12} - \frac{2C_{13}^2}{C_{33}}\right)\varepsilon_a \tag{1}$$

where ν is the Poisson ratio with a value of 0.19 [11], C_{ij} is the stiffness constants with values of $C_{11} = 345$ GPa, $C_{12} = 125$ GPa, $C_{13} = 120$ GPa, $C_{33} = 395$ GPa [12].

Fig. 1 (b) shows the variation of Raman frequencies of E_2(high) mode as a function of residual stress σ_a determined by MBE-grown samples. Here negative values of biaxial stress indicates compressive stress while positive value represents tensile one. The Raman frequency of E_2(high) mode is linearly changed with biaxial stress as shown as the red fitting line. A biaxial stress coefficient k of 2.4 ± 0.2 cm^{-1}/GPa is obtained by the best fit and strain-free Raman frequency for E_2(high) mode is determined to be 657.8 ± 0.3 cm^{-1}. The latter value coincides well with the reported value of 657.4 cm^{-1} as determined from free-standing AlN [20,21]. The $k = 2.4 \pm 0.2$ cm^{-1}/GPa is lower than previously reported 4.04 ± 0.3 and 2.9 ± 0.3 cm^{-1}/GPa, but is very close to the theoretically predicted value of 2.5 cm^{-1}/GPa [10,13,22]. With these values, residual stress of MBE-grown AlN films can be easily analyzed by Raman scattering measurement.

Let us turn to the influence of AlN buffer layer on quality improvement and their stress correlation. To improve the crystalline quality, we have used AlN buffer layers which are grown at 800 °C with a thickness of 30 nm before the growth of 360-nm-thick high temperature top layers at 950 °C. The growth rate was set at 6 nm/min, and the Al/N beam flux ratio of AlN top layer was kept as 2.9. The conditions for all AlN samples are the same except that the Al/N beam flux ratios in buffer layers are 0, 1.0, 1.2, 1.4, 1.9, and 2.4, respectively. Here the sample with an Al/N ratio of 0 means one without AlN buffer layer. As shown in Fig. 2, the two red lines represent the FWHMs of XRD ω-scans for symmetric (002) and asymmetric (102) planes of the above samples. Obviously the FWHMs values of XRD ω-scans for symmetric (002) plane are almost independent of the Al/N beam flux ratio. However, the FWHMs values of XRD ω-scans for asymmetric (102) plane become smaller with increasing the Al/N beam flux ratio. As we know, the FWHMs value of (002) XRD ω-scans refers to the density of threading dislocations with screw component while that of (102) XRD ω-scans refers to ones with edge component. Therefore, the density of edge-type threading dislocations is reduced with increasing the Al/N beam flux ratio for the AlN buffer layer growth.

To figure out why the crystalline quality could be improved with increasing Al/N beam flux ratio during the growth of buffer layer, the residual stress analysis by Raman scattering was performed. The residual stress, which was evaluated by using the obtained strain-free Raman frequency and biaxial stress coefficient above, is displayed by the blue line in Fig. 2. It is shown that all samples exhibit compressive stress and this compressive stress is reduced with increasing the Al/N beam flux ratio in the buffer layer growth. As we know, there are basically three origins for the residual biaxial stress in the AlN layer. First, the lattice mismatch between AlN and sapphire is 13%, which would lead to residual compressive stress [23]. However, it can't be the main source since the AlN layer would be quickly relaxed during the initial 6–7 monolayers growth. Second, the

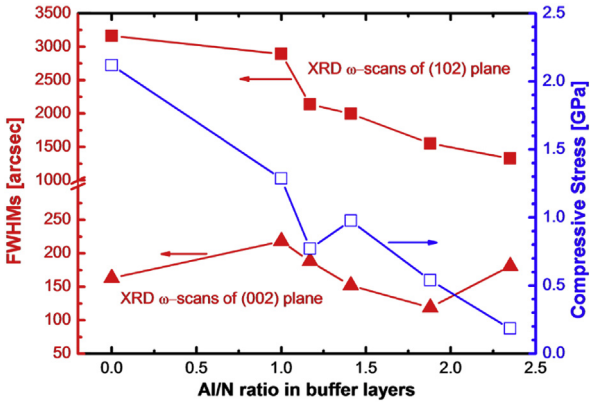

Fig. 2. Crystalline quality by XRD measurements and compressive stress status of AlN/sapphire structures at different Al/N beam flux ratio in buffer layers. The red line with solid triangles represents (002)-plane FWHMs values of XRD ω-scans, meanwhile the red line with solid squares stands for (102)-plane FWHMs values of XRD ω-scans. The blue line with open squares illustrates the compressive stress intensity. (For interpretation of the references to colour in this figure legend, the reader is referred to the web version of this article.)

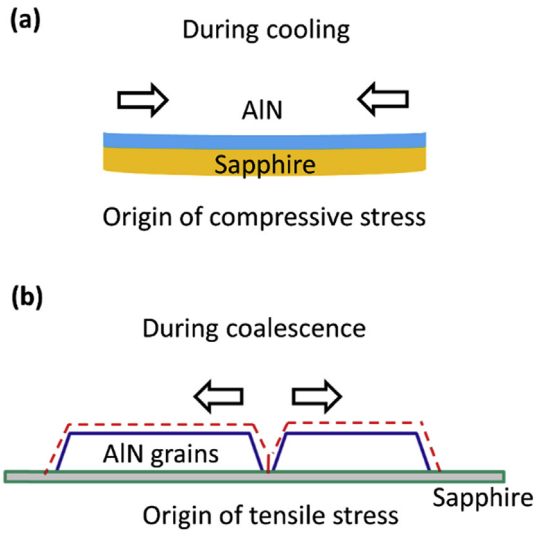

Fig. 3. The schematic diagram of the origins of compressive stress during cooling process (a) and tensile stress during coalescence one (b).

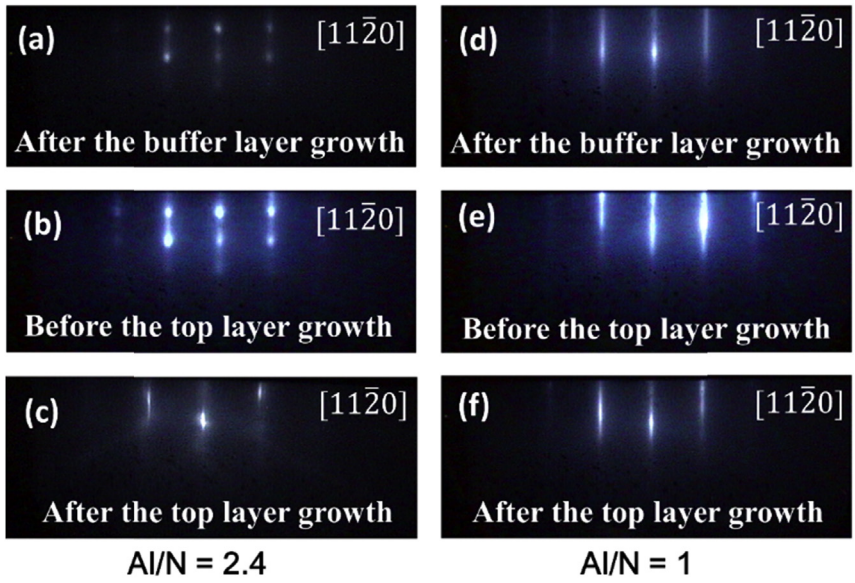

Fig. 4. RHEED patterns along [**11$\bar{2}$0**] azimuth recorded at that moment after the buffer layer growth (a)/(d), before the top layer growth (b)/(e) and after the top layer growth (c)/(f) with Al/N beam flux ratios of 2.4/1, respectively.

thermal expansion coefficient of AlN is much smaller than that of sapphire [17]. Consequently, the shrink of sapphire lattice is more intense than AlN lattice and compressive stress would be generated during cooling down of samples, as displayed in Fig. 3 (a). Third, a large number of tensile stress will be generated by the coalescence process of crystal grains during the growth or the annealing process, as demonstrated in Fig. 3 (b). Therefore, the residual stress in AlN layer mainly depends on the competition between the cooling and coalescence process. In our experiment, the compressive stress generated during sample cooling down plays a dominant role since all the samples exhibit the residual compressive strain, and the compressive stress is effectively compensated by increasing the Al/N ratio in buffer layer growth. Considering all the growth conditions are the same except the Al/N ratios, the reduction of residual compressive stress could be attributed to the increase of tensile stress generated by the improved AlN grains coalescence for higher Al/N ratio. This strong coalescence leads to the improvement of crystalline quality.

The evidence is shown in Fig. 4, which records the RHEED patterns after buffer growth, before and after top layer growth, respectively. Fig. 4 (a, b, c) present RHEED patterns of the sample buffered with Al/N beam flux ratio of 2.4, and Fig. 4 (d, e, f) present ones buffered with Al/N ratio of 1. A streaky pattern is a typical feature for 2D growth mode while spotty one is for 3D

mode. It can been seen that both samples experience the 3D growth mode at first and then are followed by the 2D growth mode. For the sample buffered with higher Al/N beam flux ratio, bigger islands were formed due to the stronger coalescence after the growth of buffer layer, leading to the maintenance of the 3D growth mode during the whole buffer layer growth process. However, as to the sample buffered with lower Al/N beam flux ratio, the coalescence of AlN grains was much weaker and the growth of buffer started in 3D mode and quickly change into 2D growth mode after 10 nm deposition of AlN buffer layer. As we know, the edge-type threading dislocations will stretch among the boundary of the islands, and the dislocation density is in reverse proportion to the size of the islands [24]. Consequently, the density of edge-type threading dislocations is decreased due to the stronger coalescence with increasing Al/N beam flux ratio during the growth of AlN buffer layer.

4. Conclusions

We have experimentally determined the strain-free Raman frequency for E_2(high) mode and biaxial stress coefficient with values of 657.8 ± 0.3 cm^{-1} and 2.4 ± 0.2 cm^{-1}/GPa, which are in good agreement with the theoretical prediction. The Raman scattering on AlN films under different Al/N beam flux ratios during the growth of AlN buffer showed that the residual compressive stress decreased with increasing Al/N beam flux ratio. *In-situ* monitoring demonstrated a stronger coalescence in AlN buffer layer during the growth for a higher Al/N ratio, resulting in the improved crystalline quality of AlN epi-layers.

Acknowledgements

This work was partially supported by the National Basic Research Program of China (No. 2012CB619300 and 2013CB632800), the National Natural Science Foundation of China (No. 61225019, 61521004, 61376060 and 61361166007) and the Open Fund of the State Key Laboratory on Integrated Optoelectronics.

References

[1] H. Hirayama, N. Maeda, S. Fujikawa, S. Toyoda, N. Kamata, Recent progress and future prospects of AlGaN-based high-efficiency deep-ultraviolet lightemitting diodes, Jpn. J. Appl. Phys. 53 (2014) 100209.
[2] M. Brendel, M. Helbling, A. Knigge, F. Brunner, M. Weyers, Solar-blind AlGaN MSM photodetectors with 24% external quantum efficiency at 0 V, Electron. Lett. 51 (2015) 1598.
[3] Z. Bryan, I. Bryan, J. Xie, S. Mita, Z. Sitar, R. Collazo, High internal quantum efficiency in AlGaN multiple quantum wells grown on bulk AlN substrates, Appl. Phys. Lett. 106 (2015) 142107.
[4] Y. Katagiri, S. Kishino, K. Okuura, H. Miyake, K. Hiramatu, Low-pressure HVPE growth of crack-free thick AlN on a trench-patterned AlN template, J. Cryst. Growth 311 (2009) 2831.
[5] R. Jain, W. Sun, J. Yang, M. Shatalov, X. Hu, A. Sattu, A. Lunev, J. Deng, I. Shturm, Y. Bilenko, R. Gaska, M.S. Shur, Migration enhanced lateral epitaxial overgrowth of AlN and AlGaN for high reliability deep ultraviolet light emitting diodes, Appl. Phys. Lett. 93 (2008) 051113.
[6] D.V. Nechaev, P.A. Aseev, V.N. Jmerik, P.N. Brunkov, Y.V. Kuznetsova, A.A. Sitnikova, V.V. Ratnikov, S.V. Ivanov, Control of threading dislocation density at the initial growth stage of AlN on c-sapphire in plasma-assisted MBE, J. Cryst. Growth 378 (2013) 319.
[7] R.G. Banal, Y. Akashi, K. Matsuda, Y. Hayashi, M. Funato, Y. Kawakami, Crack-free thick AlN films obtained by NH_3 nitridation of sapphire substrates, Jpn. J. Appl. Phys. 52 (2013) 08JB21.
[8] E. Cho, A. Mogilatenko, F. Brunner, E. Richter, M. Weyers, Impact of AlN nucleation layer on strain in GaN grown on 4H-SiC substrates, J. Cryst. Growth 371 (2013) 45.
[9] F. Demangeot, J. Frandon, M.A. Renucci, O. Briot, B. Gil, R.L. Aulombard, Raman determination of phonon deformation potentials in α-GaN, Sol. Stat. Comm. 100 (1996) 207.
[10] S. Yang, R. Miyagawa, H. Miyake, K. Hiramatsu, H. Harima, Raman scattering spectroscopy of residual stresses in epitaxial AlN films, Appl. Phys. Express 4 (2011) 031001.
[11] Y. Taniyasu, M. Kasu, T. Makimoto, Threading dislocations in heteroepitaxial AlN layer grown by MOVPE on SiC (0001) substrate, J. Cryst. Growth 298 (2007) 310–315.
[12] K. Tsubouchi, N. Mikoshiba, Zero-temperature-coefficient SAW devices on AlN epitaxial films, IEEE Trans. Sonics Ultrason. 32 (1985) 634–644.
[13] J.M. Wagner, F. Bechstedt, Phonon deformation potentials of α-GaN and-AlN: An ab initio calculation, Appl. Phys. Lett. 77 (2000) 346.
[14] A. Bhattacharyya, T.D. Moustakas, L. Zhou, D.J. Smith, W. Hug, Deep ultraviolet emitting AlGaN quantum wells with high internal quantum efficiency, Appl. Phys. Lett. 94 (2009) 181907.
[15] Y. Liao, C. Thomidis, C. Kao, T.D. Moustakas, AlGaN based deep ultraviolet light emitting diodes with high internal quantum efficiency grown by molecular beam epitaxy, Appl. Phys. Lett. 98 (2011) 081110.
[16] J.H. Pan, X.Q. Wang, G. Chen, S.T. Liu, L. Feng, F.J. Xu, N. Tang, B. Shen, Epitaxy of an Al-droplet-free AlN layer with step-flow features by molecular beam epitaxy, Chin. Phys. Lett. 28 (2011) 068102.
[17] H. Harima, Properties of GaN and related compounds studied by means of Raman scattering, J. Phys. Condens. Matter 14 (2002) R967.
[18] S. Porto, R. Krishnan, Raman effect of corundum, J. Chem. Phys. 47 (1967) 1009.
[19] T. Wermelinger, C. Borgia, C. Solenthaler, R. Spolenak, 3-D Raman spectroscopy measurements of the symmetry of residual stress fields in plastically deformed sapphire crystals, Acta. Mater 55 (2007) 4657–4665.
[20] M. Kuball, J.M. Hayes, Y. Shi, J.H. Edgar, A.D. Prins, N.W.A. van Uden, D.J. Dunstan, Raman scattering studies on single-crystalline bulk AlN: temperature and pressure dependence of the AlN phonon modes, J. Crys. Growth 231 (2001) 391.
[21] V.Y. Davydov, Y.E. Kitaev, I.N. Goncharuk, A.N. Smirnov, J. Graul, O. Semchinova, D. Uffmann, M.B. Smirnov, A.P. Mirgorodsky, R.A. Evarestov, Phonon dispersion and Raman scattering in hexagonal GaN and AlN, Phys. Rev. B 58 (1998) 12899.
[22] H.J. Trodahl, F. Martin, P. Muralt, N. Setter, Raman spectroscopy of sputtered AlN films: E_2(high) biaxial strain dependence, Appl. Phys. Lett. 89 (2006) 061905.
[23] C.J. Sun, P. Kung, A. Saxler, H. Ohsato, K. Haritos, M. Razeghi, A crystallographic model of (00•1) aluminum nitride epitaxial thin film growth on (00•1) sapphire substrate, J. Appl. Phys. 75 (1994) 3964.
[24] T. Bottcher, S. Einfeldt, S. Figge, R. Chierchia, H. Heinke, D. Hommel, J.S. Speck, The role of high-temperature island coalescence in the development of stresses in GaN films, Appl. Phys. Lett. 78 (2001) 1976.